CHAPTER 1

Introduction

The first transistor invented in 1947 by J. Bardeen and W.H. Brattain used germanium (Ge) as the semi-conducting material [1]. This opened the door to countless applications of solid state electronics. From early 1970s, microelectronics has been primarily a silicon-based technology, not only because of its high abundance in the Earth's crust but also because of the stability and high quality SiO_2 and its interface with Si substrate. The solid phase reaction at sub-eutectic temperatures between a thin metal film and a single-crystal semiconductor has attracted much interest because of its importance in Schottky barrier and contact formation, epitaxial growth and device reliability [2]. In the manufacturing of semiconductor devices and metal contacts have always played a pivotal role, especially in metal-oxide semiconductor field effect transistors (MOSFET) and complementary metal-oxide semiconductor (CMOS) devices. Contacts to ultra large scale integration (ULSI) circuits and interconnections require metal-semiconductor (MS) contacts which are thermally stable, have low resistivity and are compatible with the process technology. A good MS contact is essential for the successful operation of the electronic circuits and devices [3]. Due to the shrinking of the advanced Si-based complementary metal-oxide-semiconductor (CMOS) device feature size, it is becoming increasingly difficult to further improve Si-based CMOS performance with traditional device scaling. Thus new material and device structures to relax the physical limitation in device scaling are now required. Ge has been regarded as the replacement for Si as the channel material in future high-speed CMOS technology, due to its lower effective mass of holes [4], higher carrier mobilities [5] compared to those of Si, and its relative compatibility with silicon processing [6]. The lack of a stable native Ge oxide has been the obstacle for the use of Ge in CMOS devices [5]. However, recent developments of next generation deposited high-k dielectrics, germanium oxynitride, ZrO_2,

Al_2O_3 and HfO_2 allow for the fabrication of high performance Ge-based metal-oxide semiconductor field effect transistors (MOSFETs) [5,7]. Low reactivity with oxygen in the high-k dielectric is expected in the germanide/high-k gate stack structure [8].

Much work has been done on transition metal-Si systems but data concerning the behaviour of metal thin films on germanium upon heat treatment is relatively scarce, as little attention has been paid to transition metal-Ge systems. Therefore optimal implementation of germanium technology will require an understanding of metal-germanium interactions, from both metallurgical and electronic standpoints, and dynamic properties of process-induced defects in Ge. Most of the studies on metal-Ge reaction up to date have been carried out using in-situ annealing by slowly-ramping annealing temperature or rapid thermal annealing processing (RTP), rather than using furnace annealing, and also with less emphasis on morphological evolution.

Metal-semiconductor (MS) interfaces are an essential part of virtually all semiconductor electronic devices [9]. The MS structures are important research tools in the characterization of new semiconductor materials [10]. Their interface properties have a dominant influence on the performance, reliability and stability of device [9,11,12]. These applications include microwave field effect transistors, radio-frequency detectors, phototransistors, heterojunction bipolar transistors, quantum confinement devices and space solar cells [13,14,15,16].

The objective of this study was to add to the knowledge about: metal-germanium electrical properties and surface morphological evolution at different furnace annealing temperatures; defects induced in n-Ge during contact fabrication and annealing processes; and the temperature dependence of n-Ge Schottky diodes' electrical parameters.

An overview of the semiconductor theory with emphasis on Schottky contacts and defects is presented in Chapter 2. Chapter 3 contains the experimental details of the research. The results obtained from the study are presented in chapters 4, 5, 6, 7 and 8, while chapter 9 gives a summary and discussion of the results.

References

[1] J. Bardeen, B.W. Brattain, Phys. Rev. **74** (1948) 230.

[2] M.G. Grimaldi, L. Weiluński, M.-A. Nicolet, Thin Solid Films **81** (1981) 207.

[3] A.R. Saha, S. Chattopadhyay, C.K. Maiti, Mater. Sci. Eng. B **114-115** (2004) 218.

[4] R. Hull, J.C. Bean (Eds.), Germanium Silicon: Physics and Materials, Semiconductor and Semimetals, Vol. 56, Academics Press, San Diego, 1999.

[5] D.Z. Chi, H.B. Yao, S.L. Liew, C.C. Tan, C.T. Chua, K.C. Chua, R. Li and S.J. Lee, 7th International Workshop on Junction Technology (2007) 81.

[6] S. Gaudet, C. Detavernier, A.J. Kellock, P. Desjardins, C. Lavoive, J. Vac. Sci. Techno. A **24** (2006) 474.

[7] C.O. Chui, S. Ramanathan, B.B. Triplett, P.C. McIntyre, K.C. Saraawat, IEEE Electron Dev. Lett. **23** (2002) 473.

[8] D. Ikeno, Y. Kaneko, H. Kondo, M. Sakashita, A. Sakai,. M. Ogawa, S. Zaima, Jpn. J. Appl. Phys. **46** (2007) 1865.

[9] R.T. Tung, Mater. Sci. Eng. R **35** (2001) 1.

[10] Ö.F. Yüksel, Physica B **404** (2009) 1993.

[11] W. Mönch, Semiconductor Surf. And Interfaces, 2nd ed. Springer, Berlin 1995.

[12] S.M. Sze, Physics of Semiconductor Devices, 2nd ed. Wiley, New York, 1981.

[13] J.H. Werner, H.H. Güttler, J. Appl. Phys. **69** (1991) 1522.

[14] S. Chand, J. Kumar, J. Appl. Phys. **80** (1996) 288.

[15] K.M. Hudait, K.P. Venkateswarlu, S.B. Krupanidhi, Solid-State Electron. **45** (2001) 133.

[16] M. Soylu, B. Abay, Microelectron. Eng. **86** (2009) 88.

CHAPTER 2

THEORETICAL ASPECTS

2.1 Introduction

In this chapter, semiconductor theoretical aspects are discussed. Section 2.2 and 2.3 present the crystal and the energy band structures respectively, for germanium. Metal-semiconductor contacts are discussed in section 2.4. Section 2.5 discusses the annealing studies and germanide formation. In section 2.6 and 2.7, the fundamentals of defects in semiconductors and the theoretical aspects of deep level transient spectroscopy are presented respectively.

2.2 Crystal structure of Ge

A crystalline structure is formed when a basis of atoms is attached to every lattice point, with every basis identical in composition, arrangement, and orientation [1]. Many semiconductors have a simple crystal structure with high degrees of symmetry. Elemental and compound semiconductors have either the diamond, zinc blende, or wurzite structures. Germanium, element number 32 [2], crystallizes into the diamond structure shown in Fig. 2.1, which is actually formed by two interpenetrating face-centered cubic (fcc) lattices. The primitive basis has two identical atoms at $000;\frac{1}{4}\frac{1}{4}\frac{1}{4}$ associated with each point of the fcc lattice [1].

2.3 Band structure of Ge

The essence of energy band theories for a crystalline solid is due to the fact that many physical and optical properties of a solid can be explained using its band structure. The band structure of a crystalline solid, that is, the energy-momentum (*E-k*) relationship, is usually obtained by solving the Schrodinger equation of an approximate one-electron problem [3]. In this method the total wave functions of electrons are chosen as a linear combination of the individual wave functions in which each wave function involves only the coordinates of one

electron [4]. The Bloch theorem states that the most generalized solution for a one-electron time-dependent Schödinger equation in a periodic crystal lattice is given by [3,4]

$$\phi_k(r) = u_k(r)e^{jk.r} \tag{2.1}$$

where $u_k(r)$ is the Bloch function, which has the same spatial periodicity of the crystal potential, and $k(=2\pi/\lambda)$ is the wave vector of an electron.

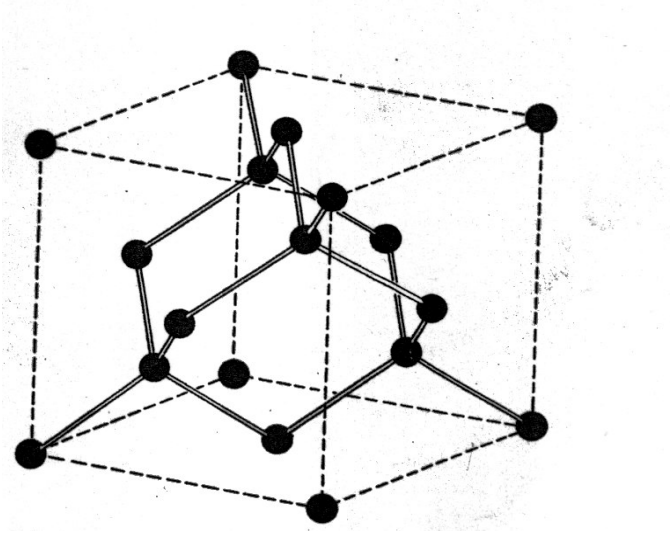

Fig. 2.1 *Crystal structure of diamond [1]*

The one-electron time-independent Schrödinger equation for which $\phi_k(r)$ is a solution can be written as [3,5]:

$$-\left(\frac{\hbar^2}{2m}\right)\nabla^2\phi_k(r) + V(r)\phi_k(r) = E_k\phi_k(r) \tag{2.2}$$

where $V(r)$ is the periodic crystal potential, which arises from the presence of ions at their regular lattice sites. From the Bloch theorem it can be shown that the energy E_k is periodic in the reciprocal lattice, and for a given band index, to label the energy uniquely, it is sufficient to use only k's in a primitive cell of the reciprocal lattice.

The energy band structures for the elemental (Si, Ge) and III-V compound semiconductors have been studied theoretically using a variety of numerical methods. The three methods most frequently used are the orthogonalized plane-wave method [6,7], the pseudopotential

method [8], and the k.p method [9]. In most cases theoretical calculations of the energy band structures for these semiconductor materials are guided by the experimental data from the optical absorption, photoluminescence and photoemission experiments [4]. For any semiconductor there is a forbidden energy region in which allowed states cannot exist. Energy bands are permitted above and below this forbidden energy region. The upper energy bands are called conduction bands and below the forbidden energy region, the valence bands. The separation between the energy of the lowest conduction band and that of the highest valence band is called the band gap E_g, which is the most important parameter in semiconductor physics. The conduction and valence bands of germanium are shown in Fig. 2.2. The Ge conduction band minimum and valence band maximum are not located at the same *k*-value, and so Ge is referred to as an indirect band gap semiconductor. The conduction band minimum of germanium crystal is located at the zone boundaries along the {111} axes. It is noted that the constant energy surfaces for electrons in germanium are ellipsoidal [4]. The value of the band gap for Ge at room temperature and under normal pressure is 0.66 eV [3].

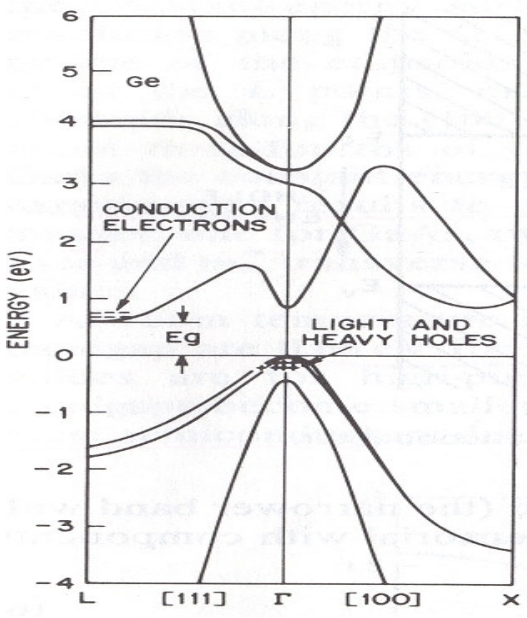

Fig. 2.2 *Energy band structure of Ge, where E_g is the energy band gap. Plus signs indicate the holes in the valence band and minus signs indicate electrons in the conduction band [1]*

The experimental results show that the band gap of Ge decreases with increasing temperature. The variation of the band gap with temperature can be expressed approximately by universal function [3]

$$E_g(T) = E_g(0) - \frac{\alpha T^2}{(T+\beta)} \tag{2.3}$$

where $E_g(0) = 1.170$ eV, $\alpha = 4.774 \times 10^{-4}$eV/K and $\beta = 235$.

Also to note is that at near room temperature, the Ge band gap increases with pressure, and its dependence on pressure is given by [3]:

$$\frac{dE_g}{dP} = 5\times 10^{-6}\ \text{eV/(kg/cm}^2) \tag{2.4}$$

2.4 Metal-semiconductor contacts

2.4.1 Introduction

Metal-semiconductor (MS) interfaces are an essential part of virtually all semiconductor electronic and optoelectronic devices [10]. The physical properties of MS interfaces are widely studied, both for their basic physical properties and for their technological applications to electronic devices [11]. The MS structures are important research tools in the characterization of new semiconductor materials [12]. Their interface properties have a dominant influence on the performance, reliability and stability of devices [3,10,13]. Electronic properties of the MS contacts are characterised by their barrier height (BH). Boyarby et al. [14] suggested that the recent motivation for studying Schottky barrier formation is due to the recognition that both electronic and chemical equilibrium have to be considered together across a reactive interface between metal and semiconductor, as surface states and metal-induced gap states failed to take into consideration the chemical equilibrium at the interface. The chemical equilibrium results in interfacial atomic rearrangement, interdiffusion, and inter-metallic compound formation, which have a profound effect on the electronic equilibrium producing the Schottky barrier [15]. Therefore, the BH is likely to be a function of the interface atomic structure, and the atomic inhomogeneities at MS interface

which are caused by grain boundaries, multiple phases, facets, defects, a mixture of different phases, etc [16,17,18,19].

2.4.2 Schottky barrier formation

When a metal is evaporated onto the surface of a semiconductor, a potential barrier is formed at the MS interface. The Fermi levels in the two materials must be coincident at thermal equilibrium. According to the Schottky-Mott model, the barrier height of an ideal metal/n-type semiconductor Schottky contact is equal to the difference between the metal work function ϕ_m (the energy required to remove an electron from the material to the vacuum level) and the electron affinity χ_s of a semiconductor (energy released when an electron is added to the material), which can be written as [20,21]

$$\phi_{Bn} = \phi_m - \chi_s \tag{2.5}$$

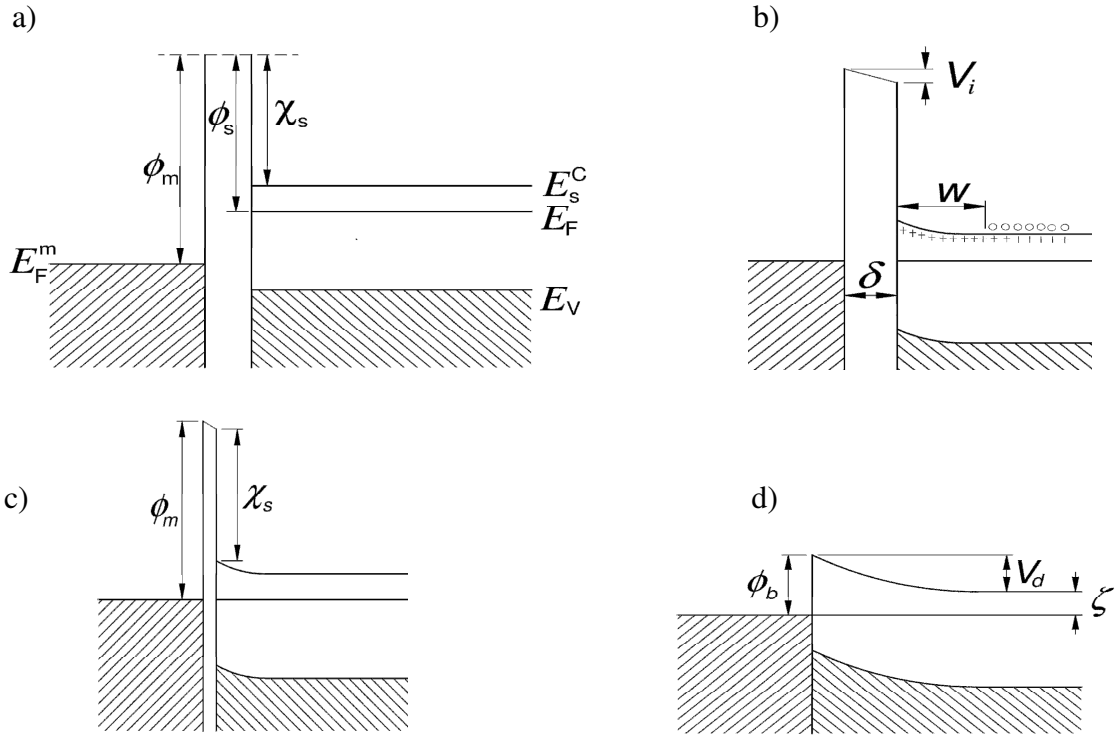

Fig. 2.3 *The formation of a Schottky barrier between a metal and a semiconductor (a) neutral and isolated states, (b) electrically connected, (c) separated by a narrow gap, and (d) in perfect contact, redrawn from ref.* 22

Fig. 2.3 shows the formation of a Schottky barrier. Part (a) shows the metal and the semiconductor in their isolated, electrically neutral states for an n-type semiconductor with work function ϕ_s less than that of the metal, which, in practice, is the most important case. If the semiconductor and metal are connected by means of a wire, electrons pass from the semiconductor to the metal. Due to the flow of the electrons, there must be a negative charge on the surface of the metal and a positive charge builds up on the surface of the semiconductor, resulting an electric field in the gap between the metal and the semiconductor. The equilibrium condition is established when the Fermi levels of the two materials coincide as illustrated in Fig. 2.3 (b).

The negative charge on the surface of the metal consists of extra conduction electrons contained within the Thomas-Fermi screening distance of about 0.5 Å. Because the semiconductor is n-type, the positive charge will be provided by conduction electrons moving from the surface leaving uncompensated positive donor ions in a region depleted of electrons. Due to the fact that the donor concentration is much lower than the concentration of electrons in the metal, the uncompensated donors occupy a layer of appreciable thickness w. The potential changes slowly over the depletion region, and results in bands bending downwards as shown in Fig. 2.3 (b). The difference between the electrostatic potentials outside the surface of the metal and semiconductor is given by $V_i = \delta E_i$, where δ is their separation and E_i is the electric field in the gap. As the metal and semiconductor approach each other, the electric field stays finite (Fig. 2.3 (c)), and results in V_i tending to zero as the gap diminishes. When the metal and semiconductor finally touch (Fig. 2.3 (d)), the barrier due to the vacuum disappears completely, and the only barrier seen by electrons, is that resulting from the bending of the bands in the semiconductor.

As shown in Fig. 2.3 (d), the height of the barrier relative to the position of the conduction band in the neutral region of the semiconductor is called the diffusion potential (also called the built-in-potential), V_d can be expressed by

$$V_d = \phi_{Bn} - \xi \tag{2.6}$$

where ξ is the Fermi (or chemical) potential of an n-type semiconductor (the energy difference between the Fermi level and conduction band) and is given by [3]

$$\xi = kT \ln\left(\frac{N_C}{N_D}\right) \tag{2.7}$$

where N_C is the density of states in the conduction band of the semiconductor, N_D is the doping density, k is the Boltzmann constant and T is the Kelvin temperature.

2.4.3 Schottky barrier behaviour under forward and reverse bias

A Schottky barrier diode is a majority-carrier device, as the current flow in such a device is due to the majority carriers (e.g electrons in an n-type semiconductor). Under zero bias conditions, electrons from both the semiconductor and the metal see the same barrier height relative to their Fermi levels. Therefore, there is no net flow of electrons over the barrier in either direction.

Applying a bias voltage to the contact so that the metal is positive, the bands in the semiconductor are raised in energy compared to those in the metal, causing the electric field in the barrier to decrease. The decrease in electric field takes place within the semiconductor barrier region and shape of the barrier changes as illustrated in Fig. 2.4 (a). The diffusion potential V_d is decreased compared to the zero-bias condition. The electrons can now cross from the semiconductor to the metal more easily as they now see a reduced barrier. However, if a positive potential is applied to the semiconductor, the Fermi level of the semiconductor is lowered relative to that of the metal, and the diffusion potential V_d is increased (Fig. 2.4 (b)), resulting in the number of electrons able to surmount the barrier into the metal decreasing. This also increases the width of the depletion region. Therefore, in the reverse biased mode, very little current flows through the device.

2.4.4 Depletion layer

For the determination of the spatial distributions of potential and electric fields, the depletion layer width, and the junction capacitance of a Schottky diode, a Poisson's equation in the space-charge region has to be solved using proper boundary conditions.

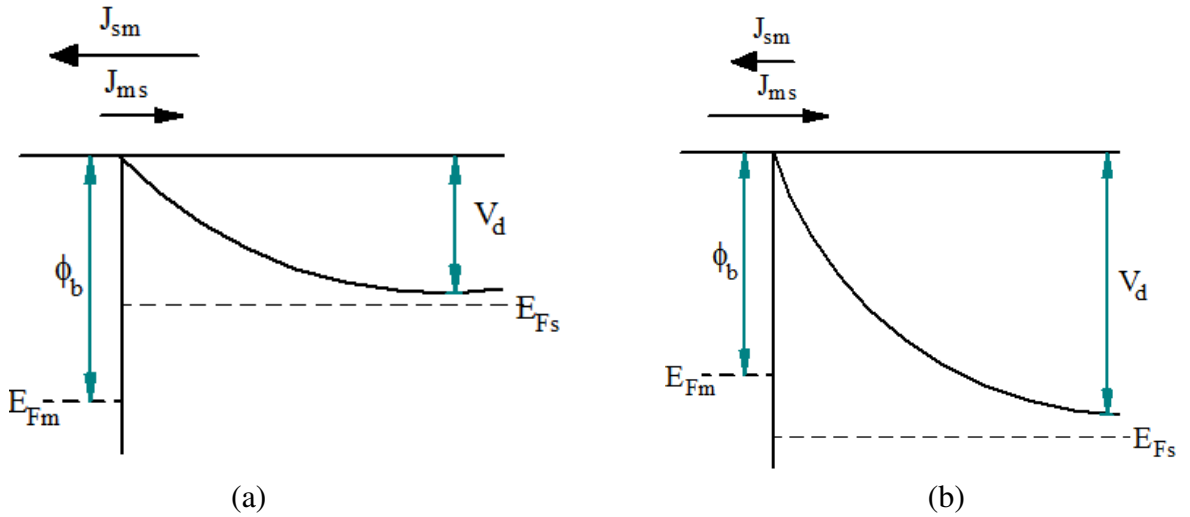

Fig. 2.4 *Schottky barrier (a) under forward bias, (b) under reverse bias, redrawn from ref. 22.*

The boundary conditions are obtained from the barrier height, and that there is no electric field in the bulk of the semiconductor. Considering that $x = 0$ at the interface, the boundary conditions can be written as $V(0) = V_d$ and $E(\infty) = 0$, where V is the contact potential and E is the electric field. The Poisson's equation in the depletion region of a Schottky diode can be written as

$$\frac{d^2V}{dx^2} = \frac{1}{\varepsilon_s}\rho(x) \tag{2.8}$$

where $\rho(x)$ is the total charge density in the semiconductor at depth x and ε_s is the permittivity of the semiconductor. In general, $\rho(x)$ should include contributions from valence band, conduction band, ionized donors and acceptors, and deep levels in the band gap. This will result to a complicated equation that can only be solved by numerical methods. The equation can be simplified by applying the depletion approximation. By using the depletion or abrupt approximation, it is assumed that the semiconductor can be divided into two regions: the depletion region, directly below the metal, which contains no free carriers, and the bulk of the semiconductor, which is electrically neutral and in which the electric field is zero. In the depletion region, as there are no electrons in the conduction band, the charge density $\rho(x)$ is qN_D. If the width of the depletion region is w, the charge density in the semiconductor can be written as

$$\rho(x) = \begin{cases} qN_D & if\ x \le w \\ 0 & if\ x > w \end{cases} \tag{2.9}$$

where N_D is the density of dopants and q is the electronic charge.

By integrating Eq. (2.8) twice and applying the boundary condition, the depletion width can be written as

$$w = \sqrt{\frac{2\varepsilon_s V_d}{qN_D}} \tag{2.10}$$

When the contact is biased by an externally applied voltage V_a, the depletion width can be expressed as

$$w = \sqrt{\frac{2\varepsilon_s}{qN_D}\left(V_d - V_a - \frac{kT}{q}\right)} \tag{2.11}$$

where the term $\frac{kT}{q}$ arises from the contribution of the majority-carrier distribution tail (electrons in the n side). It is seen from Eq. (2.11) that the depletion layer width is directly proportional to square root of applied voltage and is inversely proportional to the square root of the dopant density of the semiconductor. The electric field and the potential in the depletion region are given respectively by

$$E(x) = \frac{qN_D}{\varepsilon_s}(x - w) \tag{2.12}$$

and

$$V(x) = -\left(\frac{qN_D}{\varepsilon_s}\right)\left(\frac{x^2}{2} - wx\right) - \phi_{Bn} \tag{2.13}$$

Fig. 2.5 shows a graph of $\rho(x)$, $E(x)$, and $V(x)$ for a Schottky barrier.

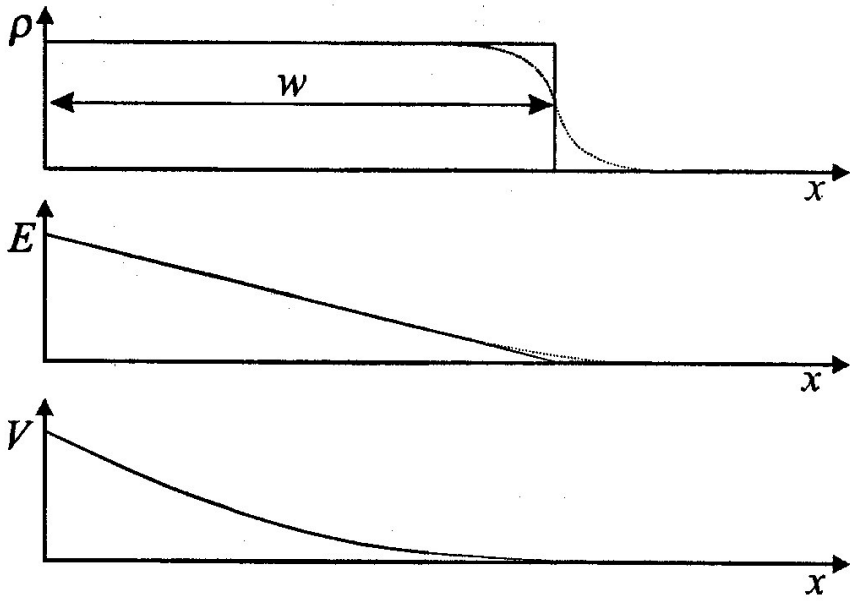

Fig. 2.5 *Graphs of the charge density $\rho(x)$, electric field E and electrostatic potential V.*

The space charge density Q_{sc} per unit area of the semiconductor and depletion layer capacitance C per unit area are given by

$$Q_{sc} = qN_D w = \sqrt{2q\varepsilon_s N_D (V_d - V_a - \frac{kT}{q})} \tag{2.14}$$

$$C = \frac{\partial Q_{sc}}{\partial V} = \sqrt{\frac{q\varepsilon_s N_D}{2(V_d - V_a - kT/q)}} = \frac{\varepsilon_s}{w} \tag{2.15}$$

Eq. (2.15) can also be expressed in the form,

$$\frac{1}{C^2} = \frac{2(V_d - V_a - kT/q)}{q\varepsilon_s N_D} \tag{2.16}$$

or

$$N_D = \frac{2}{q\varepsilon_s}\left[-\frac{1}{d(1/C^2)/dV}\right] \tag{2.17}$$

If N_D is constant throughout the depletion region, a straight line should be obtained by plotting $1/C^2$ versus V. If N_D is not constant, the differential capacitance method can be used to determine the doping profile from Eq. (2.17). From the intercept on the voltage axis, the barrier height can be determined:

$$\phi_{Bn} = V_i + \xi + \frac{kT}{q} - \Delta\phi \tag{2.18}$$

where V_i is the voltage intercept, and ξ is the depth of the Fermi level below the conduction band, which can be computed if the doping concentration is known and $\Delta\phi$ is the image force barrier lowering and is given by

$$\Delta\phi = \left[\frac{qE_m}{4\pi\varepsilon_s\varepsilon_0}\right]^{1/2} \tag{2.19}$$

with E_m being the maximum electric field and being given by

$$E_m = \left[\frac{2qN_DV_i}{\varepsilon_s\varepsilon_0}\right]^{1/2} \tag{2.20}$$

2.4.5 Image-force lowering of the barrier

When an electron is at a distance x from the metal, a positive charge will be induced on the metal surface. The force of attraction between the electron and the induced positive charge is equivalent to the force that would exist between the electron and the image charge located at $-x$. The image force is given by

$$F = \frac{-q^2}{16\pi\varepsilon_s x^2} \tag{2.21}$$

where ε_s is the permittivity of the semiconductor. The work done by an electron due to its transfer from infinity to the point x is given by

$$V(x) = \int_{\infty}^{x} F dx = \frac{q^2}{16\pi\varepsilon_s x}. \tag{2.22}$$

The energy above corresponds to the potential energy of an electron at distance x from metal surface, shown in Fig. 2.6, and is measured downwards from the x axis. When an external field E is applied, the total potential energy PE is given by

$$PE(x) = \frac{q^2}{16\pi\varepsilon_s x} + qEx \tag{2.23}$$

The maximum potential energy occurs at a position x_m where the resultant electric field is zero; i.e. the field due the image force is equal and opposite to the field in the depletion region, or

$$\frac{q}{16\pi\varepsilon_s x_m^2} = E_m \tag{2.24}$$

where E_m is the maximum electric field. As a result of the image force, the maximum potential in the barrier is lowered by an amount

$$\Delta\phi = x_m E_m + \frac{q}{16\pi\varepsilon_s x_m} = 2x_m E_m = \sqrt{\frac{qE_m}{4\pi\varepsilon_s}} \tag{2.25}$$

The value ε_s may be different from the semiconductor static permittivity, as during the emission process, the electron transit time from metal-semiconductor interface to the barrier maximum x_m is shorter than the dielectric relaxation time, the semiconductor medium does not have enough time to be polarized, and smaller permittivity than the static value is expected [3].

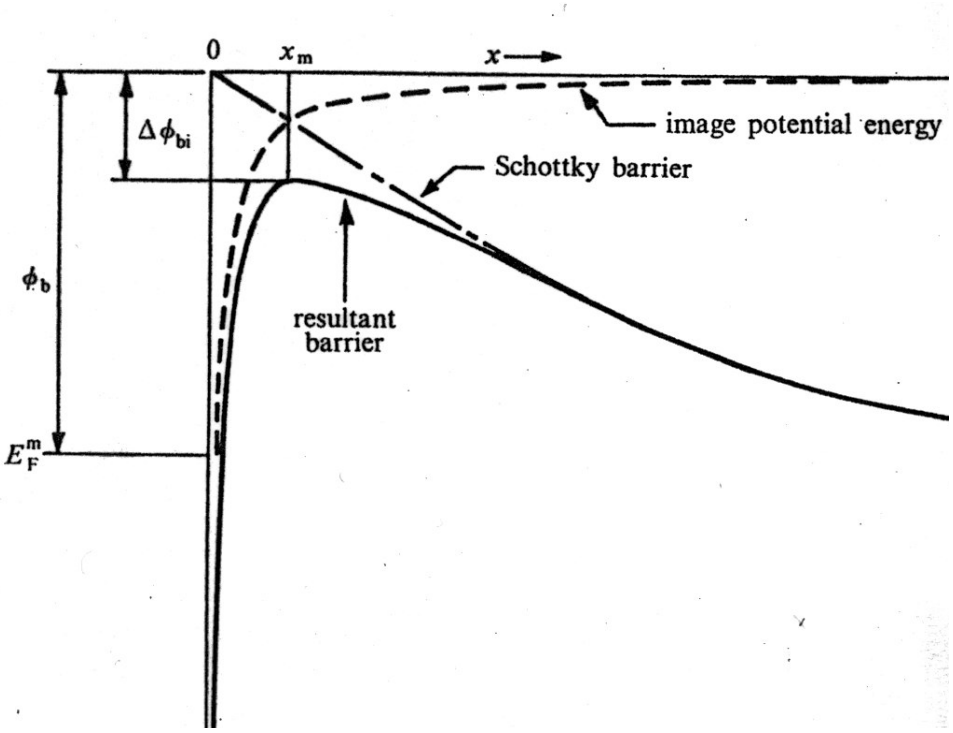

Fig. 2.6 *Image-force lowering of barrier, redrawn from ref. 22.*

2.4.6 Ohmic contact

An ohmic contact is a metal-semiconductor contact that has a negligible contact resistance R_c, relative to the bulk of the semiconductor. The contact resistance is defined as the reciprocal of the derivative of current density with respect to voltage. When evaluated at zero bias the contact resistance is given by

$$R_c = \left(\frac{\partial J}{\partial V} \right)_{V=0}^{-1}. \tag{2.26}$$

A satisfactory ohmic contact should not significantly perturb device performance, and it can supply the required current with a voltage drop that is sufficiently small compared with the drop across the active region of the device [3]. To achieve ohmic contacts to semiconductors, for an *n*-type semiconductor, the metal work function, ϕ_m must be less than that of the semiconductor ϕ_s as depicted in Fig. 2.7 (a) and (b), and ϕ_m must be greater than ϕ_s in case of a *p*-type semiconductor. For an n-type semiconductor at equilibrium, electrons are transferred from the metal to the semiconductor, resulting in the aligning of the Fermi Levels.

This raises the semiconductor energy bands, reducing the barrier to electron flow between the metal and semiconductor.

A more practical ohmic contact is a tunnel contact, shown in Fig. 2.7 (c). Such contacts have a high doping in the semiconductor such that there is only a thin barrier separating the metal from the semiconductor, and carriers can easily tunnel across the barrier. The doping density to achieve a tunnel contact should be 10^{19} cm^{-3} or higher.

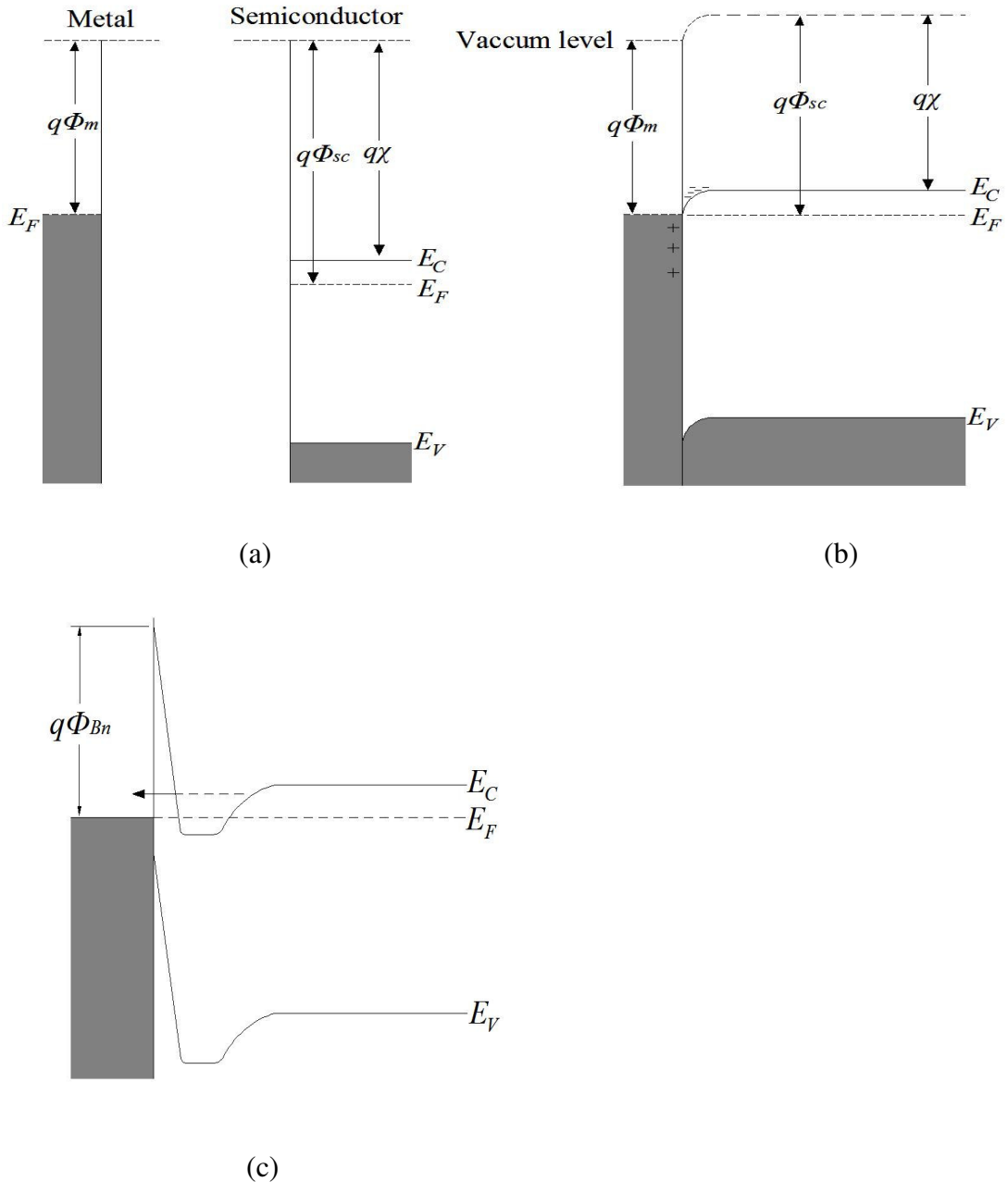

Fig. 2.7 *Energy band diagrams of a metal/n-type semiconductor with* $\Phi_m < \Phi_{sc}$.

2.4.7 Current transport mechanisms

The current transport in metal-semiconductor contacts is mainly due to majority carriers, unlike in p-n junction, where the minority carriers are responsible. There are four main mechanisms by which carrier transport can occur in Schottky barriers in forward biased direction [3]. The transport mechanisms are shown in Fig. 2.8. The mechanisms are:

A: thermionic emission over the potential barrier into the metal,

B: quantum-mechanical tunnelling through the barrier (important for heavily doped semiconductors and responsible for most ohmic contacts),

C: recombination and/or generation in the space charge region, and

D: hole injection from the metal to the semiconductor (equivalent to recombination in the neutral region).

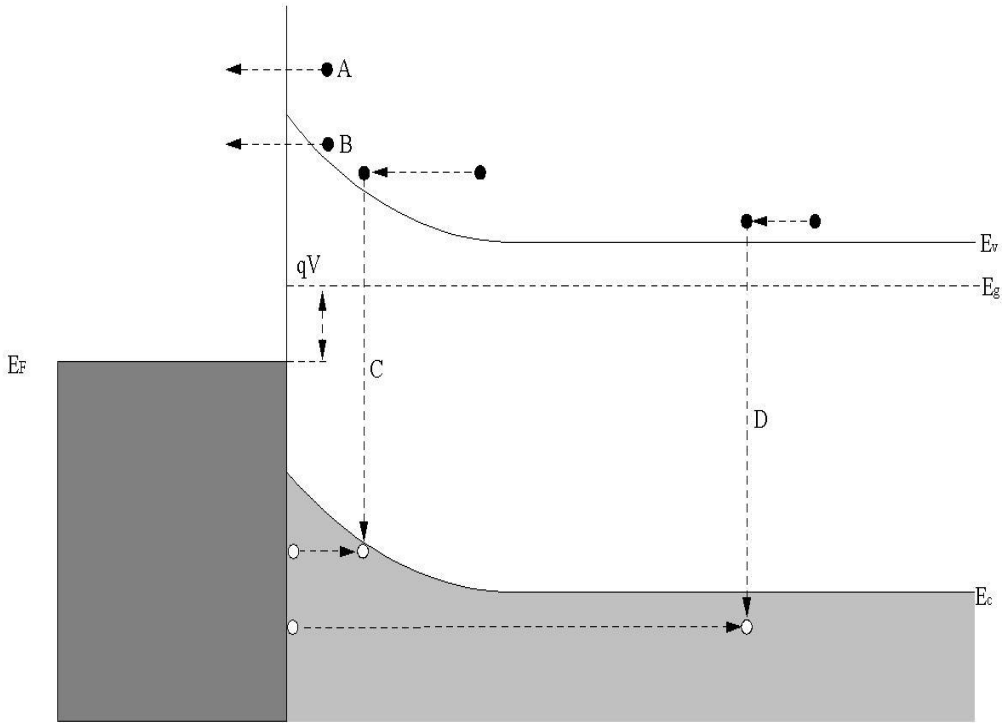

Fig. 2.8 *Current transport mechanisms redrawn from ref. 22.*

2.4.7.1 *Thermionic emission current.*

This mechanism is dominant for Schottky diodes with moderately doped semiconductors operated at moderate temperatures (e.g. 300 K) [3]. Emission of electrons over the barrier into the metal are governed by two basic processes, (i) electrons are transported from the interior of the semiconductor to the interface by the mechanism of drift and diffusion in the electric field of the barrier, and (ii) at interface, their emission into the metal is determined by the rate of transfer of electrons across the boundary between the metal and the semiconductor. These two processes are effectively in series, and the current is determined predominantly by whichever causes the larger impediment to the flow of electrons [22]. For high-mobility semiconductors (e.g. Si and Ge) the current transport can be described by the thermionic emission theory by Bethe [23] using the assumptions that the barrier height ϕ_{Bn} is much larger than kT, thermal equilibrium established at the plane that determines emission, and the existence of a net current flow does not affect thermal equilibrium so that one can superimpose two current fluxes. Because of these assumptions, the shape of the barrier profile is immaterial and current flow depends solely on the barrier height [3]. The current density $J_{s\to m}$ from the semiconductor to the metal can be expressed as:

$$J_{s\to m} = \int_{E_F+q\phi_B}^{\infty} qv_x dn \tag{2.27}$$

where $E_F + q\phi_B$ is the minimum energy required for thermionic emission into metal, and v_x is the carrier velocity in the direction of transport. The electron density can be expressed in an incremental range as:

$$dn = N(E)F(E)dE$$

$$= \frac{4\pi(2m^*)^{\frac{3}{2}}}{h^3}\sqrt{E-E_c}\exp[-(E-E_c+qV_n)/kT]dE \tag{2.28}$$

where $N(E)$ and $F(E)$ are the density of states and the distribution function, respectively; m^* is the effective mass of the semiconductor; and qV_n is $(E_C - E_F)$.

Postulating that all the energy of electrons in the conduction band is kinetic energy, then

$$E - E_C = \frac{1}{2} m^* v^2$$

$$dE = m^* v dv$$

$$\sqrt{E - E_C} = v\sqrt{m^*/2}. \tag{2.29}$$

Substituting Eq. (2.29) into Eq. (2.28) results

$$dn = 2\left(\frac{m^*}{h}\right)^3 \exp\left(-\frac{qV_n}{kT}\right)\exp\left(\frac{-m^* v^2}{2kT}\right)(4\pi v^2 dv) \tag{2.30}$$

Eq. (2.30) gives the number of electrons per unit volume with speeds between v and $v + dv$ distributed over all directions [3]. Resolving the speed into components along the axes with the x axis parallel to the transport direction, we have

$$v^2 = v_x^2 + v_y^2 + v_z^2 \tag{2.31}$$

With the transformation $4\pi v^2 dv = dv_x dv_y dv_z$ we obtain from Eqs. (2.27), (2.30) and (2.31)

$$J_{s\to m} = \left(\frac{4\pi q m^* k^2}{h^3}\right) T^2 \exp(-\frac{qV_n}{kT})\exp\left(-\frac{m^* v_{ox}^2}{2kT}\right) \tag{2.32}$$

where v_{ox} is the minimum velocity required in the x direction to surmount the barrier and is given by

$$\frac{1}{2} m^* v_{ox}^2 = q(V_d - V) \tag{2.33}$$

where V_d is the built-in potential at zero bias. Substituting Eq. (2.33) into (2.32) we get

$$J_{s\to m} = \left(\frac{4\pi q m^* k^2}{h^3}\right) T^2 \exp\left(-\frac{q(V_n + V_d}{kT}\right)\exp\left(\frac{qV}{kT}\right)$$

$$= A^{*}T^{2}\exp\left(-\frac{q\phi_B}{kT}\right)\exp\left(\frac{qV}{kT}\right) \tag{2.34}$$

where ϕ_B is the barrier height and equals the sum of V_n and V_d , and

$$A^{*} = \frac{4\pi q m^{*} k^{2}}{h^{3}} \tag{2.35}$$

is the effective Richardson constant for thermionic emission.

Since the barrier height for electrons moving from the metal into the semiconductor remains the same, the current flowing into the semiconductor is thus unaffected by the applied voltage [3]. It must therefore be equal to the current flowing from the semiconductor into the metal when equilibrium prevails (i.e., when $V = 0$). The corresponding current density at equilibrium is

$$J_{m\to s} = -A^{*}T^{2}\exp\left(-\frac{q\phi_B}{kT}\right) \tag{2.36}$$

The total current density is given by the sum of Eqs.(2.34) and (2.36).

$$J_n = \left[A^{*}T^{2}\exp\left(-\frac{q\phi_B}{kT}\right)\right]\left[\exp\left(\frac{qV}{kT}\right)-1\right]$$

$$= J_{ST}\left[\exp\left(\frac{qV}{kT}\right)-1\right] \tag{2.37}$$

where J_{ST} is the saturation current density given by

$$J_{ST} = A^{*}T^{2}\exp\left(-\frac{q\phi_B}{kT}\right) \tag{2.38}$$

Eq. 2.37 is the current density of an ideal diode. For a non-ideal diode, the series resistance R_s, and the ideality factor, n need to be factored into Eq. (2.37). The resulting expression becomes,

$$J_n = J_{ST} \exp\left[\frac{q(V - IR_s)}{nkT}\right]\left(1 - \exp\left[-\frac{q(V - IR_s)}{kT}\right]\right) \tag{2.39}$$

The ideality factor is obtained as the gradient of the slope of the linear region of the semi logarithmic *I-V* plot and is given by [3]

$$n = \frac{q}{kT}\left(\frac{dV}{d(\ln I)}\right) \tag{2.40}$$

2.4.7.2 *Quantum-mechanical tunnelling.*

This is usually the dominant transport mechanism in a heavily doped semiconductor at low temperatures. The current in the forward direction arises from the tunnelling of electrons with energies close to the Fermi energy in the semiconductor. This is known as 'field' emission [22]. If the temperature is raised, electrons are excited to higher energies and tunnelling probability increases very rapidly because the electrons 'see' a thinner and lower barrier. Although the number of excited electrons decrease very rapidly with increasing energy, there is a maximum contribution to the current from electrons which have energy well above the bottom of the conduction band. This mechanism is known as thermionic-field emission. When the tunnelling current dominates the current flow, the transmission coefficient is given by [3]

$$T(\eta) \approx \exp\left(-\frac{q\phi_B}{E_{00}}\right) \tag{2.41}$$

where E_{00} is the characteristic energy level given by

$$E_{00} = \frac{q\hbar}{2}\sqrt{\frac{N_D}{\varepsilon_s m^*}} \tag{2.42}$$

The tunnelling current density is given by

$$J_t = \exp\left(-\frac{q\phi_B}{E_{00}}\right) \tag{2.43}$$

2.4.7.3 *Generation recombination current.*

This mechanism is as a result of the generation and recombination of carriers within the space charge region. The recombination normally takes place via localized centres, and the most effective centres are those with the energies lying near to the centre of the gap. The theory of the current due to such a recombination centre is the same for a Schottky diode as for p-n junction [22], and the current density is given by

$$J_r = J_{r0}\exp\left(\frac{qV}{2kT}\right)\left[1-\exp\left(-\frac{qV}{kT}\right)\right] \tag{2.44}$$

where $J_{r0} = qn_i w/2\tau_r$, n_i is the intrinsic electron concentration, proportional to $\exp(-qE_g/2kT)$, w is the depletion width and τ_r is the lifetime within the depletion region. The two main processes for recombination are direct and indirect recombination [24]. In the direct recombination process, an electron falls from the conduction band and recombines directly with a hole in the valence band. This is also called band to band recombination. This process is common as radiative transitions in direct bandgap semiconductors. For this process energy is conserved as the electrons and holes recombining are located close to the band edges of the semiconductor. In indirect recombination, an electron falls into a trap where it can later recombine with a hole.

2.4.8 Barrier height determination

The Schottky barrier height of a metal-semiconductor contact can be determined by current – voltage (*I-V*) and the capacitance-voltage (*C-V*) measurement techniques. First, considering the *I-V* measurement technique, the barrier heights are deduced from the *I-V* characteristics, which are analysed by the thermionic emission model given by the Eq. (2.37). The extrapolated value of current at zero voltage in the semi-log forward bias *ln I-V* characteristics is the saturation current I_o, and the barrier height can be obtained from the equation

$$\phi_{Bn} = \frac{kT}{q}\ln\left(\frac{A^* AT^2}{I_0}\right) \tag{2.45}$$

where A is the diode effective are.

The barrier height can also be determined using the capacitance-voltage measurement technique. In this technique, the concept of the induced or image charge in the metal and semiconductor is used. To use this type of method for barrier height determination, it must be assumed that the diode should be nearly ideal such that the doping concentration remains uniform in the semiconductor. From the plot of $1/C^2$ *vs* V, the barrier height can be calculated as given in Eq. (2.18).

2.4.9 Barrier height inhomogeneities

The most interesting form of Schottky barrier height (SBH) inhomogeneity is the presence of small regions of the metal-semiconductor interface with a low SBH, embedded in an interface with an otherwise uniform high SBH [25]. This will result in the lateral variations of the electrostatic potential at the interface, causing the current to flow preferentially through the lower barriers in the potential distribution [26]. Assuming a Gaussian distribution of the inhomogeneous barrier heights with a mean value $\bar{\phi}_B$ and a standard deviation σ_s in the form [27]:

$$P(\phi_B) = \frac{1}{\sigma_s \sqrt{2\pi}} \exp\left(\frac{(\phi_B - \bar{\phi}_B)^2}{2\sigma_s^2} \right) \tag{2.46}$$

where $1/\sigma_s \sqrt{2\pi}$ is the normalization constant. The total current $I(V)$ is given by [27]

$$I(V) = \int_{-\infty}^{+\infty} I(\phi_B, V) P(\phi_B) d\phi \tag{2.47}$$

On integration

$$I(V) = A^* A T^2 \exp\left(-\frac{q\phi_{ap}}{kT} \right) \exp\left(\frac{qV}{n_{ap} kT} \right) \left[1 - \exp\left(-\frac{qV}{kT} \right) \right] \tag{2.48}$$

with

$$I_0 = A^* A T^2 \exp\left(-\frac{q\phi_B}{kT} \right) \tag{2.49}$$

where I_0 is the saturation current, ϕ_{ap} and n_{ap} are the apparent barrier height and apparent ideality factor at zero bias respectively:

$$\phi_{ap} = \bar{\phi}_{B0(T=0)} - \frac{q\sigma_{s0}^2}{2kT} \tag{2.50}$$

and

$$\left(\frac{1}{n_{ap}} - 1\right) = \rho_2 - \frac{q\rho_3}{2kT} \tag{2.51}$$

It is also assumed that the standard deviation σ_s and the mean value of the Schottky barrier height $\bar{\phi}_B$ are linearly bias-dependent on Gaussian parameters that are given by $\bar{\phi}_B = \bar{\phi}_{B0} + \rho_2 V$ and $\sigma_s = \sigma_{s0} + \rho_3 V$, where ρ_2 and ρ_3 are the voltage coefficient that may depend on temperature (T) and they quantify the voltage deformation of the barrier height distribution [27,28]. The decrease of zero-bias barrier height is caused by the existence of the Gaussian distribution and the extent of influence is determined by the standard deviation itself [26,27]. The effect is particularly significant at low temperatures, as at low temperatures, charge carriers have very low energies to surpass the barrier, tunnelling of electrons is the dominant process. Because the barrier is non-homogeneous, further tunnelling through the low barrier regions cause the deviation of the barrier height from the value that could be obtained for a uniformly distributed barrier at the metal-semiconductor interface [29]. From Eq. (2.50), the plot of ϕ_{ap} versus 1000/T should be a straight line giving $\bar{\phi}_{B0}$ and σ_{s0} from the intercept and slope respectively. The standard deviation is a measure of the barrier homogeneity. The lower the value of σ_{s0} corresponds to a more homogeneous barrier height and better diode rectifying properties.

Following the barrier height inhomogeneities correction, the Richardson plot is modified by combining Eqs. (2.49) and (2.50):

$$\ln\left(\frac{I_0}{T^2}\right) - \left(\frac{q^2\sigma_{s0}^2}{2k^2T^2}\right) = \ln(A^{**}A) - \frac{q\bar{\phi}_{B0}}{kT} \tag{2.52}$$

where A^{**} is the modified Richardson constant. A plot of the modified $\ln\left(\frac{I_0}{T^2}\right)-\left(\frac{q^2\sigma_{s0}^2}{2k^2T^2}\right)$ versus 1000/T yields a straight line with the slope giving the mean barrier height and the intercept giving the modified Richardson constant.

2.5 Annealing studies and germanides formation

Annealing is a heat treatment wherein a material is altered, causing changes in its properties [30]. Isothermal annealing is when the heat treatment is carried out at a constant temperature, and isochronal annealing, is when the heat treatment is carried out at constant time duration. Annealing occurs by the diffusion of atoms within a solid material, so that the material progresses towards its equilibrium state. To avoid oxidation, annealing is carried out in Ar gas. The solid state reaction at subeutectic temperatures between a thin metal film and a single-crystal semiconductor has attracted much interest because of its importance in Schottky barrier and contact formation, epitaxial growth and device reliability [31]. Inter-diffusion, contaminations, chemical reaction, compound formation, interface roughening, defect generation, dopant migration, etc. can all be derived by thermodynamics due to the thermal annealing [32]. It is well known that the chemical reactions between metals and semiconductors at an interface can play an important role in the electrical properties of devices. During the annealing process, metals may react with germanium and new compounds (germanides) would form, resulting in the change of barrier heights. Hence, the change of barrier heights may be attributed to the combined effects of interfacial reaction and phase transformation [33]. Thermal degradation at high annealing temperatures includes two mechanisms: agglomeration and phase transformation [34]. Agglomeration starts with grain boundary grooving and results in islands formation. Agglomeration is driven by the minimization of the total surface/interface energy of the germanide and germanium substrate [35]. In this work, the effects of thermal treatment on the electrical and morphological evolution characteristics of metal germanides at different annealing temperatures were investigated.

2.6 Fundamentals of defects in semiconductors

2.6.1 Introduction

It is generally known that a perfect crystal lattice does not exist in real crystals. Defects or imperfections are always found in all crystalline solids. The existence of defects has a profound effect on the physical properties of a crystal. These imperfections may introduce electronic energy states into the semiconductor bandgap, either as shallow levels or deep levels. Shallow level defects are located near the valence band for acceptors and conduction band for donors. These shallow levels, which are ionized at room temperature, are normally created by impurity elements used as dopants in semiconductors and provide free carriers to form *p*-type or *n*-type semiconductor. Deep level defects are those found deeper in the band gap than dopant levels. The deep levels do not contribute much to the free charge carriers, as they have higher ionization energies. The deep level defects act either as traps or as recombination centres in the semiconductors, depending on the capture cross section of the electrons and holes [36]. The semiconductor free carrier density is reduced by traps, whereas recombination centres introduce generation-recombination currents in rectifying devices. In the electronic industry the trap-induced carrier reduction is utilised to form areas of high resistivity for device isolation [36]. Depending on the application, these defects may either be beneficial or detrimental for optimum device functioning [37]. The discussion in this section is more focused on the vacancy defects, interstitial defects, the *E*-centre and the *A*-centre.

2.6.2 Vacancy Defect

A vacancy defect (V) is created when an atom moves out of its regular site, and is shown in Fig. 2.9. A vacancy lattice site is considered as the simplest of all defects [38]. In some semiconductors (e.g. Ge), the vacancy can have up to five charge states, V^{++}, V^{+}, V^{0}, V^{-} and $V^{=}$.

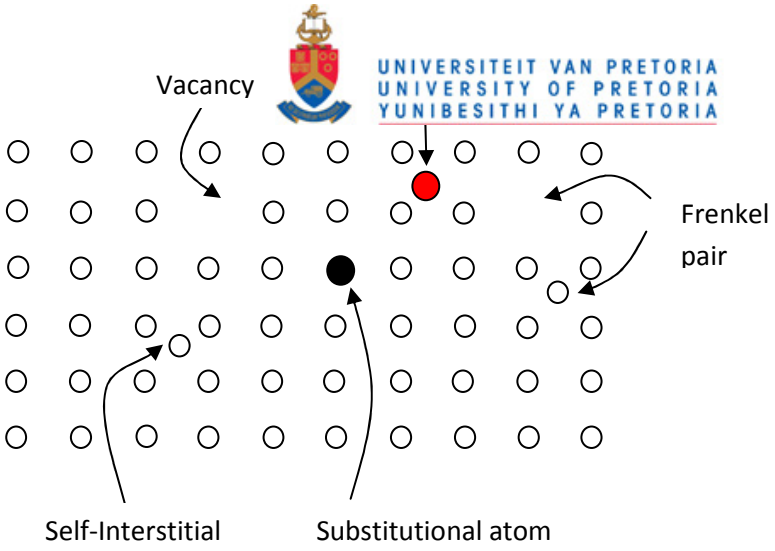

Fig. 2.9 *Schematic representation of the vacancy, Interstitial and Substitutional defects*

Fig. 2.10 (a) depicts a vacancy defect in a diamond lattice. In order to form a vacancy, four bonds are broken. The broken bonds (dangling) bonds can form new bonds leading to atomic displacements [39]. The number of electrons which occupy these dangling bonds depend on the charge state of the vacancy. These small atomic displacements of the neighbours of the vacancy can be inward or outward displacements, which may either, preserve the local symmetry (relaxation) or alter it (distortion). The amplitude of these displacements as well as the new symmetry depends on the type of the bonding [39]. The split-vacancy is shown in Fig. 2.10 (b), where a one neighbour of the vacancy is displaced half way between its original position and the centre of the vacancy. This configuration is also known as the saddle-point configuration for vacancy migration in the diamond lattice. The split-vacancy is often important primarily to help describe the transition state in vacancy migration [40]. The divacancy results from the removal of two neighbouring atoms. In general the divacancies can be created in semiconductors by particle irradiation either as a primary defect (when collision casacade is dense enough) or as a secondary defect by pairing of single vacancies diffusing randomly.

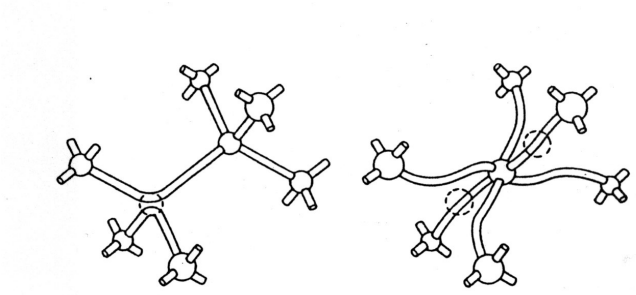

(a) (b)

Fig. 2.10 *Configuration of (a) the vacancy in a diamond lattice and (b) the saddle-point.*

2.6.3 Interstitial Defect

An interstitial defect is due to an atom occupying a site in the crystal structure, which is not its regular lattice site as depicted in Fig. 2.9. It can be of the same species as the atoms of the lattice or of different species (interstitial impurity). The energy of formation of an interstitial defect is higher than the corresponding energy for a vacancy. The introduction of interstitial results in large lattice strain, and the motion of such defect reduce this strain; hence interstitial occurs more readily than a vacancy. In radiation damage, interstitials and vacancies occur in equal numbers, and more often the interstitial is associated with a nearby vacancy, the vacancy having resulted from the same collision event. This Frenkel or interstitial-vacancy pair can be taken as a single defect.

2.6.4 The E-centre and A-centre

The *E*-centre or vacancy-donor pair is the dominant defect produced in electron- or gamma-irradiated float zone silicon, oxygen lean silicon-germanium and germanium [41]. The *E*-centre results from a vacancy trapped next to a substitutional donor atom. It can form either as a primary defect or when the impurity atom captures a mobile vacancy. It has been found that the *E*-centre has at least three charge states in Ge: the double negative, the single negative, and the neutral [42]. For the V-Sb pair, the ionization enthalpy of the double-acceptor is $\Delta H_{na} = 0.377$ eV as determined by reverse biasing DLTS [43,44], and that of the single acceptor is $\Delta H_{pa} = 0.307$ eV as determined by forward-pulsing DLTS [43,44]. The *A*-centre or vacancy-oxygen complex is produced when a vacancy is trapped next to an oxygen atom in an interstitial position. Also an *A*-centre defect can be formed as a primary defect or when an oxygen impurity traps a mobile vacancy. The *A*-centre defect concentration is dependent on the O impurity concentration in the sample. The *A*-centre is a dominant defect induced by irradiation with high energy particles (electrons, protons, etc) in Si crystals grown by the Czochralski method [45] and oxygen-rich Ge crystals [46]. In Si the *A*-centre is known to exist in two charge states: singly negatively charged and neutral with the corresponding acceptor level at about E_c-0.17 eV [46,47]. It was argued in Refs. [48,49] that the *A*-centre in Ge has three charge states, double negative (VO^{--}), singly negative (VO^{-}) and neutral (VO^{0}) and confirmed by Markevich et al. [46] that the E_cń 0.21 eV and E_v+0.27 eV traps in Ge are related to (--/-) and (-/0) levels of the *A*-centre.

2.7 Aspects of Deep Level Transient Spectroscopy

2.7.1 Introduction

Deep levels are quantum states which are within the forbidden bandgap of the semiconductor; deep levels influence the electrical and the optical properties of semiconductor materials. Since deep level defects can be detrimental to or enhance the operation of devices fabricated on semiconductors, it is important to know the electrical properties of these deep levels. Many processes that occur in deep levels are nonradiative, and therefore cannot be observed by optical techniques. Deep level transient spectroscopy (DLTS) is one of the techniques used to determine the electrical properties of deep defects.

2.7.2 Deep level transient spectroscopy

In this study, deep level transient spectroscopy (DLTS) was used to evaluate and characterise the electrically-active defects induced in Ge Schottky contacts during contact fabrication and annealing processes. This is a powerful and sensitive high-frequency capacitance transient thermal scanning technique, which is useful for observing traps in semiconductors. This technique was developed by Lang [50] in 1974, and it monitors the change in capacitance of the depletion layer of a p-n junction or Schottky diode as a result of charge transfer between the deep levels and conduction or valence bands. It displays the spectrum of traps in a crystal as positive and negative peaks on a flat baseline as a function of temperature. The sign of the peak shows whether the deep level is near the valence band or conduction band, the height of the peak is proportional to the trap concentration, and the position, in temperature, of the peak is determined by the thermal emission properties of the trap [50]. Furthermore, one can measure the activation energy, and electron- and hole-capture cross sections for each trap.

2.7.3 Emission and capture of carriers by trapping centres

Whenever the thermal equilibrium condition of a system is perturbed, there are processes that take place to restore the system to equilibrium. This may involve the emission and capture of the electrons and holes. A defect level is defined as an electron trap as one which tends to have deficiency of electrons, and thus capable of capturing them from the conduction band. Likewise, a hole trap is one which is full of electrons, and thus capable of having a trapped electron recombining with a hole [50]. An electron trap occurs when the electron capture rate

c_n from the conduction band is much larger than the hole capture rate c_p from the valence band, i.e. $c_n >> c_p$, and a hole trap has to have $c_p >> c_n$. A recombination centre is one for which c_n and c_p are almost similar, i.e. $c_n \approx c_p$. Fig. 2.11 depicts the four common processes that a deep level (E_T) can interact with the conduction band and the valence band. If the trap is neutral it may capture an electron from the conduction band (Fig. 2.11 (a)), characterized by c_n. After an electron capture, one of the two events can take place, the centre can either emit the electron back to the conduction band, i.e. electron emission e_n (Fig. 2.11 (b)), or it can capture a hole from the valence band, depicted in Fig 2.11 (c) as c_p. Similarly for a hole trap, occupied by a hole, either it emits the hole back to the valence band e_p in Fig 2.11 (d) or captures an electron (Fig. 2.11 (a)).

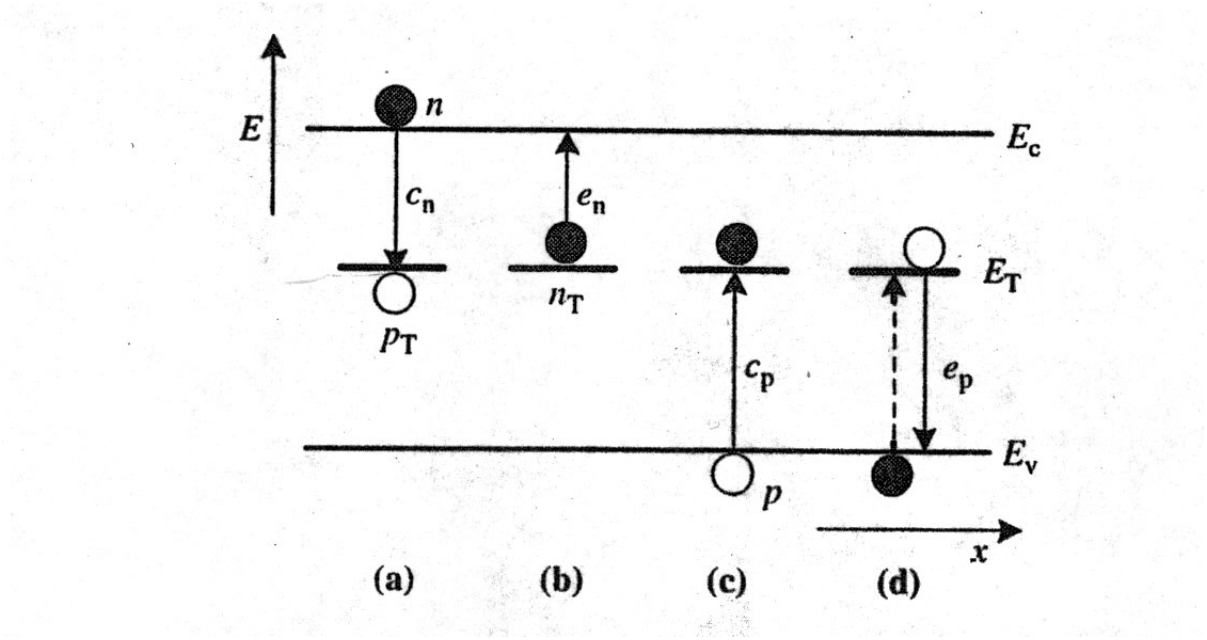

Fig. 2.11 *Emission and capture processes involved by trapping at a deep level E_T.*

Shockley et al. [51], Hall [52] and Bourgoin et al. [53], have extensively discussed the kinetics of emission and capture of carriers from defect levels. The electron and hole capture rates are given by:

$$c_n = \sigma_n < v_n > n, \tag{2.53}$$

$$c_p = \sigma_p < v_p > p, \tag{2.54}$$

where σ_n and σ_p are defect's capture cross-sections for capturing electrons and holes respectively, and n is the electron concentration, p is the hole concentration and $<v_n>$ is the average electron thermal velocity:

$$< v_n >= \sqrt{\left(\frac{3kT}{m^*}\right)} \tag{2.55}$$

where m^* is the effective mass of the electron, k is the Boltzmann constant, and T is the temperature in Kelvin. A similar equation can be written for v_p. The thermal emission rate e_n, of electrons deep level to the conduction band is proportional to the Boltzmann factor $\exp(-E_T/kT)$, and can be written as [54,55]

$$e_n(T) = \frac{\sigma_n < v_n > N_C}{g} \exp\left[-\frac{\Delta E_T}{kT}\right] \tag{2.56}$$

where $\Delta E_T = E_C - E_T$, is the activation energy of the defect level, g is the degeneracy of the defect level, T is the temperature in Kelvin, N_C is the effective density of states in the conduction band given by

$$N_C = 2M_C\left(\frac{2\pi m^* kT}{h^2}\right)^{\frac{3}{2}} \tag{2.57}$$

where M_C is the number of conduction-band minima, h is Planck's constant. The emission rate for holes is also expressed in an analogous way.

If the capture cross-section of the defect is assumed to be independent of temperature, the product $< v_n > N_C$ in Eq. (2.56) has T^2 dependence. It follows that an Arrhenius plot of $\ln\left(\frac{e_n}{T^2}\right)$ as a function of $\frac{1}{T}$ should be a linear relationship from which the defect's energy E_T and capture cross-section σ_n may be determined. These two parameters are referred to as the defect's signature. The defect signature is one of the essential parameters used to identify a defect during electrical characterization. If the capture cross-section is assumed to be temperature-dependent, it takes the form [56]:

$$\sigma_n(T) = \sigma_\infty \exp\left(\frac{\Delta E_\sigma}{kT}\right) \tag{2.58}$$

where σ_∞ is the capture cross-section extrapolated to $T = \infty$ and ΔE_σ is the thermal activation energy of the capture cross-section (i.e. thermal barrier for carrier capture). The temperature dependence of a capture cross-section may be determined from the plot of $\ln(\sigma_n)$ versus $\frac{1}{T}$, where ΔE_σ is extracted from the slope and σ_∞ after extrapolation to $T = \infty$. The corrected activation energy for a deep level which exhibits a temperature-dependent capture cross-section is given by

$$\Delta E_a = \Delta E_T + \Delta E_\sigma \tag{2.59}$$

A more general expression of the thermal emission rate can now be written as,

$$e_n(T) = \frac{\sigma_n < v_n > N_C}{g} \exp\left[-\frac{\Delta E_T + \Delta E_\sigma}{kT}\right] \tag{2.60}$$

The parameter ΔE_T, is the Gibbs free energy change for the ionization of the state given by [57]

$$\Delta E_T = \Delta H - T\Delta S \tag{2.61}$$

where ΔH and ΔS are the changes in enthalpy and entropy due to the change in charge state of the level. Substituting Eq. (2.61) into 2.56 yields

$$e_n(T) = \frac{\sigma_n < v_n > N_C}{g} \exp\left[-\frac{\Delta S}{k}\right] \exp\left[-\frac{\Delta H}{kT}\right] \tag{2.62}$$

Therefore, the Arrhenius plot yields the activation enthalpy of the deep level, and not the free energy, which can only be determined from the optical measurements [54,55].

2.7.4 Capacitance transient

The DLTS technique uses a fast, sensitive capacitance meter to measure the capacitance of a reverse-biased Schottky, MOS or p-n junction [50]. This discussion is limited to Schottky barrier diodes. The capacitance of a reverse-biased diode is related to the width of the depletion region (Eq. (2.15)), which also depends on the charge in the depletion region

(Eq. (2.11)), due to dopants as well as deep defects. When a reverse bias is applied to the metal-semiconductor system, a space-charge region is created i.e. region depleted of mobile free carriers. In this space-charge region there are ionised impurities. If the trapped charges in deep levels, in this space-charge region can be altered then the occupancy can be detected by monitoring the junction capacitance.

Consider a Schottky diode on an *n*-type semiconductor, as shown in Fig. 2.12 (1), with an electron trap which introduces a deep level trap E_T . The deep levels under the Fermi level are assumed to be filled and those above are empty as governed by the Fermi distribution function. In Fig. (2.12), shaded and open circles indicate filled and empty traps respectively.

At the start of the DLTS cycle, a majority carrier filling pulse is applied across the diode (Fig. 2.12 (2)). This pulse will collapse the space-charge region, increasing the capacitance of the Schottky diode drastically, and trapping electrons in those levels that are now below the Fermi level. After the filling pulse is removed, the reverse bias is returned to its quiescent level (Fig. 2.12 (3)). The increase in the reverse bias increases the width of the depletion region again. Since some of the deep level traps in the space-charge region are filled, the charge density in the space-charge region is less than it was in Fig. 2.12 (1). Therefore the depletion width is slightly wider and the capacitance slightly lower than it was in (1). This excess charge in the space-charge region may be transferred to the conduction band through the emission process as depicted in Fig. 2,12 (4), causing the charge density in the depletion region to increase, reducing its width and increasing the capacitance of the junction. The density of occupied defect levels at time t after removing the filling pulse is given by [55].

$$N(t) = N_T \exp(-e_n t) \tag{2.63}$$

where e_n is the electron thermal emission rate and N_T is the defect concentration. If it is assumed that $N_T << N_D$, there will not be much change in the depletion width during the emission of carriers. Therefore it is assumed that the emission of carriers from the space-charge region may be described by an exponential decay (Eq. (2.63)). The capacitance of the Schottky diode is assumed to have the form:

$$C(t) = C_\infty - \Delta C \exp(-e_n t) \tag{2.64}$$

where $C(t)$ is the capacitance transient at time t, C_∞ is the quiescent reverse bias capacitance at time $(t) = \infty$ and ΔC is the difference between C_∞ and the capacitance measured at $(t) = 0$. The concentration of a specific trap can be determined from the change in capacitance as a function of the region being sampled. If the carrier charge density N_D and trap level concentration N_T are spatially uniform, and N_T is much lower than N_D, then the defect concentration is given by the following approximation

$$N_T \approx 2N_D \frac{\Delta C}{C} \tag{2.65}$$

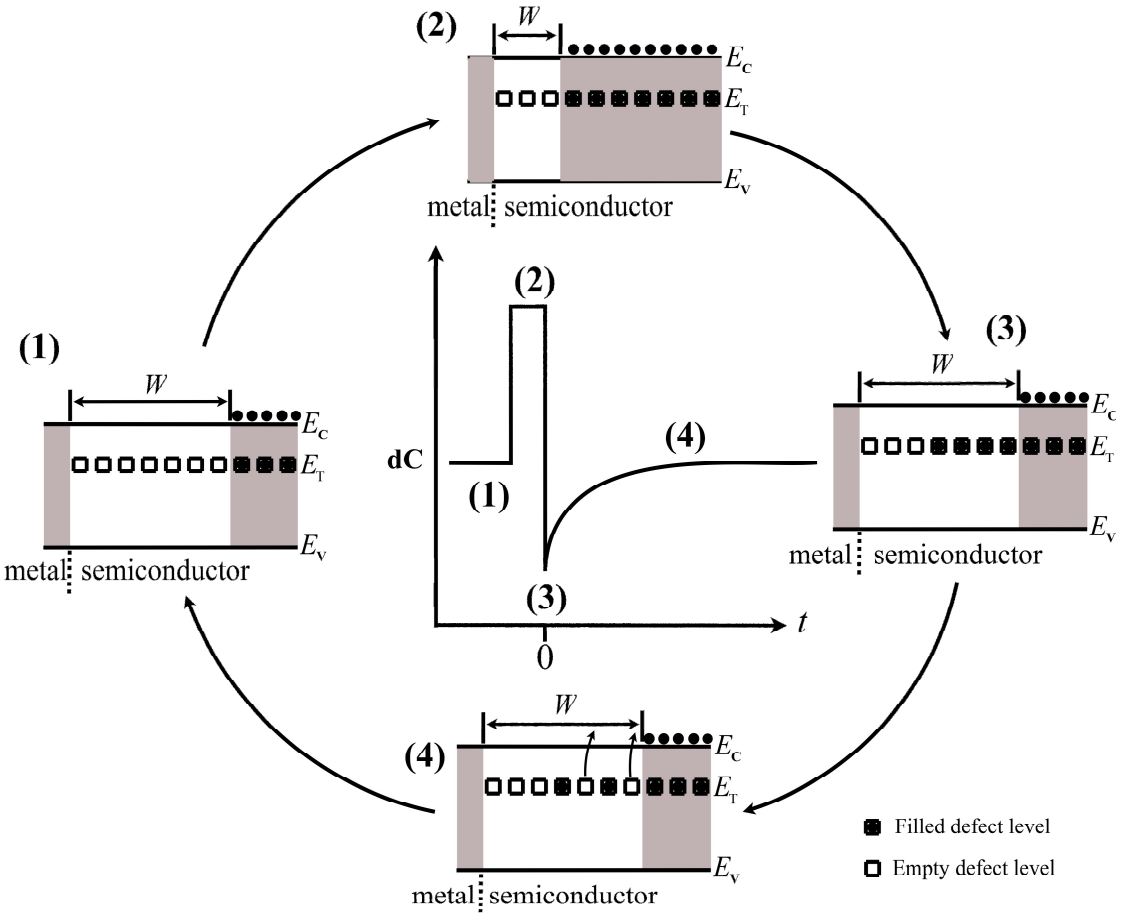

Fig. 2.12 *The capacitance transient due to an electron trap in n-type material. (1): Quiescent state, (2): Filling pulse, (3) Reverse bias; (4) Exponential decay as carriers are emitted.*

2.7.5 Principles of DLTS

Lang [50] introduced the 'rate window' concept to deep level characterization. The measurement system produces a maximum output only when a transient with a rate within this narrow window occurs. As the emission rate is strongly temperature dependent, a thermal scan only reveals the presence of different traps at characteristic temperature when their emission rates coincide with the rate window. Also the maximum signal output is proportional to the defect concentration. Early DLTS systems employed the dual-gated (double boxcar) signal filter for determining the rate window and averaging transients to enhance the signal-to-noise ratio (SNR) of the output, enabling detection of low concentration defects [50,54]. The DLTS signal is obtained from the difference between the capacitance measured at time t_2 and the capacitance at time t_1 and produces an output proportional to their average difference. As depicted in Fig. 2.13 (a), at low temperature there is a slow transient, such that the DLTS signal $S = C(t_1) - C(t_2)$ is very low. As the temperature is increased, the transient decay rate increases causing a greater change in the capacitance between times t_1 and t_2, and resulting in the DLTS signal increase. This increase in DLTS signal continues until the transient decays so fast that most of the decay occurs before t_1. A further increase in time will now decrease the DLTS signal. Fig. 2.13 (b) shows a peak that is observed when the DLTS signal is plotted as a function of temperature. The time constant at which the maximum DLTS signal is observed is given by:

$$\tau_{\max} = \frac{t_1 - t_2}{\ln\left(\frac{t_1}{t_2}\right)} \tag{2.66}$$

In most of the modern analogue DLTS systems, a lock-in amplifier is used to analyse the DLTS transient. In a lock-in amplifier set-up, response to the transient is the integral product of the capacitance signal and the weighting function $w(t)$ given by

$$S(\tau) = \frac{1}{\tau}\int_0^{\tau} C(t)w(t)dt \tag{2.67}$$

where $w(t) = \sin\left(\frac{2\pi t}{\tau}\right)$ is a sine wave of fixed frequency.

The result obtained is the same as that obtained from the double boxcar method. Since the lock-in amplifier method uses more of the signal, therefore it is less sensitive to noise than the double boxcar method. For an exponential transient with a sine wave weighting function, the DLTS signal reaches a maximum when $\lambda = \left(\frac{1}{0.423\tau}\right)$.

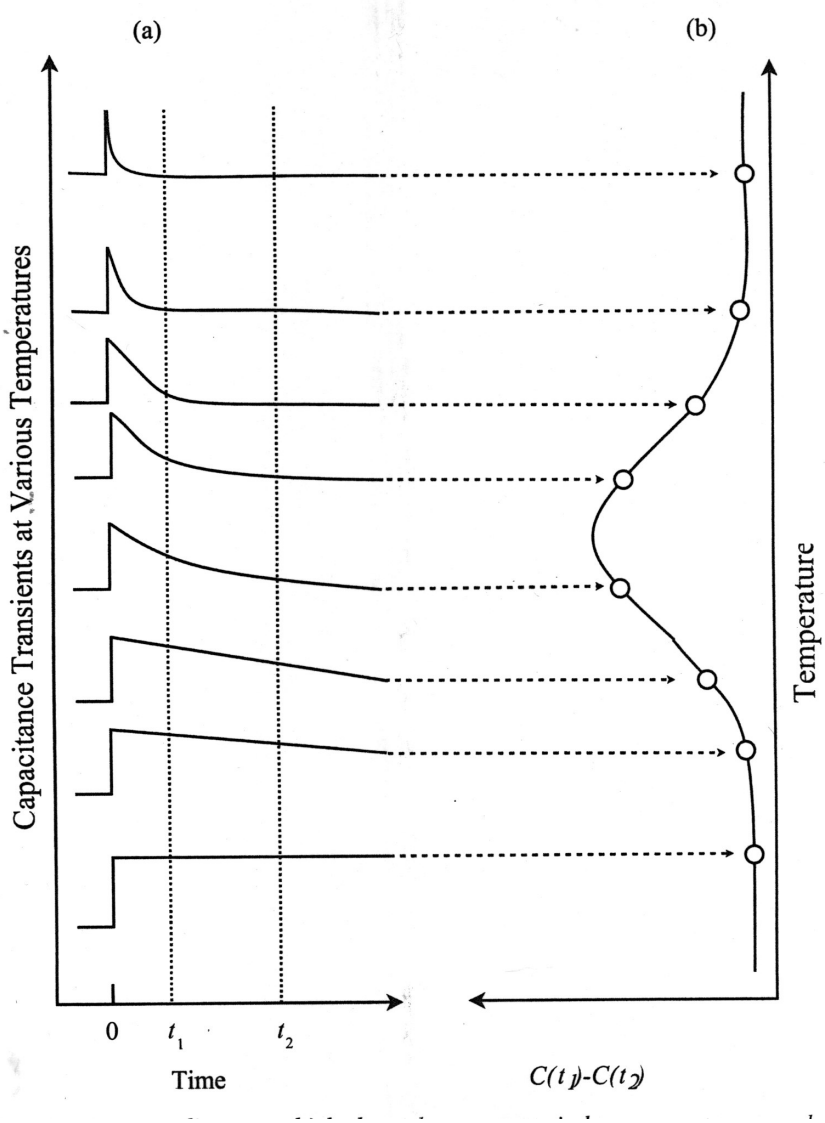

Fig. 2.13 *(a) The change in capacitance transient with increasing temperature and (b) the DLTS signal obtained from the transients plotted as a function of temperature, after ref. 50.*

2.7.6 *Defect depth profiling*

The concentration of deep levels is given in Eq. (2.65). This equation is only applicable if the minority carrier pulse or majority carrier pulse is large and long enough to completely fill the trap and $\Delta C << C$. The appropriate pulse for deep level concentration determination can be checked by making several scans with increasing larger and longer pulses, until the deep level peak no longer increase in size. Lang [50] has reported that, using Eq. 2.65, N_T is underestimated, especially for thin films and at low reverse bias voltage. In order to find the corrected expression for N_T one has to consider the region λ, where the deep level crosses the Fermi level a distance λ shallower than the depletion region edge as depicted in Fig. 2.14. The traps in this region are occupied and do not contribute to capacitance change when filling pulse is applied. The width of this region is given [58].

$$\lambda = \left(\frac{2\varepsilon (E_F - E_T}{q^2 N_D} \right)^{\frac{1}{2}} \tag{2.68}$$

where ε is the semiconductor dielectric constant E_F is the Fermi level and q is the electronic charge. The depth profiling technique uses a fixed bias voltage and a variable filling pulse [59]. In this method, the incremental change in capacitance $\delta(\Delta C)$ is monitored as the majority carrier pulse V_P is varied by a small amount δV_P. The relative incremental change in capacitance due to the pulse increment is given by [58].

$$\delta\left(\frac{\Delta C}{C}\right) = \left(\frac{\varepsilon}{qw^2 N_D}\right)\frac{N_T(x)}{N_D(x)}\delta V_P \tag{2.69}$$

where x is the depth below the junction, N_D is the ionized shallow impurity concentration and w is the depletion width, corresponding to a steady-state reverse biased condition.

The carrier charge density $N_D(x)$ is obtained from $C-V$ measurements, and the corrected deep level concentration can be expressed as [58];

$$N_T = \frac{2\Delta C(0) N_D(x)}{C}\left[\left(\frac{x-\lambda}{x}\right)^2 - \left(\frac{x_p - \lambda_p}{x}\right)^2\right]^{-1} \tag{2.70}$$

where $x-\lambda$ and $x_p-\lambda_p$ are the depletion region width before and after applying a filling pulse respectively and λ_p is the value of λ during the pulse. Values of 10^{-5}-10^{-6} for $\frac{\Delta C}{C}$ can be achieved in the low noise measurements and a low defect concentration of the order 10^{10} cm^{-3} is detectable if the shallow dopants concentration is $N_D \approx 10^{16}$ cm^{-3}.

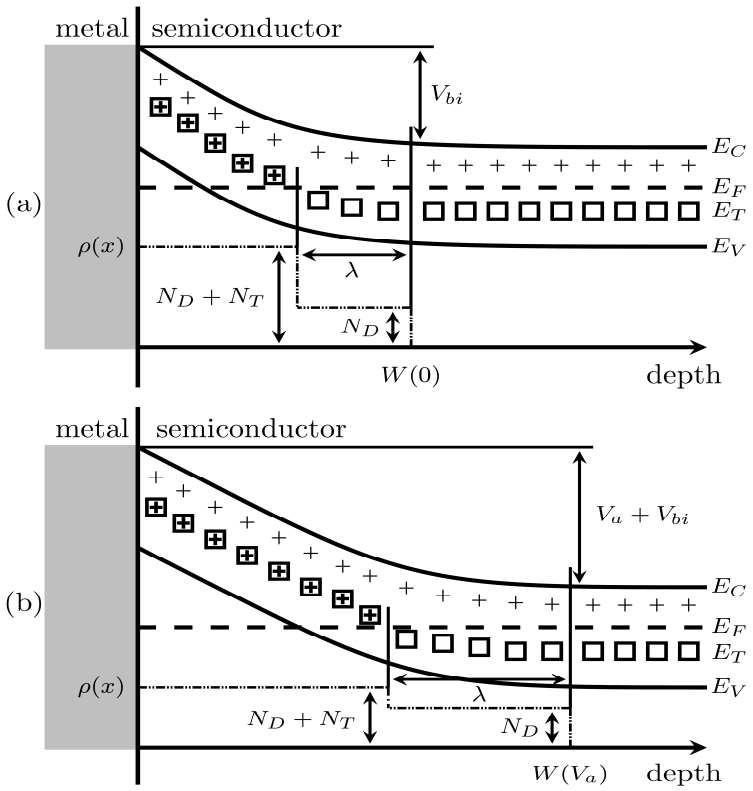

Fig. 2.14 *Energy band diagram, the λ and space charge for an n-type metal-semiconductor junction with deep levels for unbiased and after applying a quiescent reverse bias of V_a (after ref. 58)*

2.7.7 Principles of Laplace-DLTS

DLTS technique has limitations in separating closely spaced transients due to its poor emission rate and time constant resolution. In 1990, Dobaczewski et al [56,60] developed an improved high-resolution version of DLTS, called Laplace-DLTS (LDLTS).

Generally, there are two DLTS classes of transient processing methods, which are analog and digital signal processing. Analog signal processing is carried out in real-time process which involves extracting the capacitance transients as temperature is ramped. The output produced

by an analog filter will be proportional to the signal input within a particular time constant range. The digital signal processing digitizes the analog transient output of the capacitance meter and averages many of these digitized transients to reduce noise. The concept of digitizing capacitance at constant temperature and extracting the time constant is the basis of high resolution of LDLTS. A numerical algorithm is employed to extract all accessible time constants from the transients.

For the quantitative description of non-exponential behaviour in the capacitance transients, we need to assume that the recorded transients *f(t)* are characterized by a spectrum of emission rates [61]

$$f(t) = \int_0^\infty F(s)e^{-st}ds \tag{2.71}$$

where *f(t)* is the Laplace transform of the true spectral density *F(s)*. To determine a real spectrum of emission rates in the transient, an inverse Laplace transform for the function *f(t)* should be performed, producing a spectrum of delta-like peaks for multi-, mono-exponential transients.

LDLTS gives an intensity output as a function of emission rate. The area under each peak is related to the initial trap concentration. The measurement is carried out at a fixed temperature, and capacitance transients are recorded and averaged. LDLTS provides an order of magnitude higher energy resolution than the conventional DLTS technique [61]. Consequently, LDLTS can separate states with very similar emission rates.

2.7.8 Field dependence of the emission rate

Although it is often assumed that the electric field affecting deep levels in the space-charge region is negligible, there is strong evidence that in some cases the emission rate does depend upon the applied bias and doping. The electric field will distort the shape of the potential well. This distortion of the potential well may enhance the emission probability of a carrier trapped in the well, adversely affecting the accurate determination of defect concentration [62], as saturation of the defect peak amplitudes may occur depending on the effect of the electric field on the emission of electrons from the defect. Pons et.al [63], have reported that the DLTS signal of a defect that saturates quickly with an increase in filling pulse amplitude has an emission rate that depends strongly on electric field strength in the space-charge

region. The influence of the electric field can affect the emission process in different ways, as depicted in Fig. 2.15. The most well known emission enhancement mechanism is the Poole-Frenkel mechanism [64]. This mechanism enhances the emission rate of a defect by lowering the deep level potential. The Poole-Frenkel effect leads to a decrease (ΔE_{PF}) of the ionisation energy (ΔE_T) of a coulombic well placed in an electric field F , and

$$\Delta E_{PF} = \sqrt{\frac{qF}{\pi\varepsilon}} \tag{2.72}$$

where ε is the dielectric constant of the material and q the electron charge.

When substituted in Eq. 2.56, the emission rate of the defect is now given by

$$e_n^{'} = e(0)\exp\left(\frac{1}{kT}\sqrt{\frac{qF}{\pi\varepsilon}}\right) \tag{2.73}$$

where $e(0)$ is the emission rate at zero electric field, k is the Boltzmann's constant and T is the absolute temperature.

The dependence of the emission rate ($e_n^{'}$) on electric field F for a coulombic well, i.e. $\ln(e_n^{'})$ proportional to $F^{\frac{1}{2}}$, has been used as experimental evidence to distinguish between donor and acceptor defects. The linearity of this dependence shows a charge leaving a centre of opposite sign. This implies a donor type trap in *n*-type material and acceptor type defect in *p*-type material.

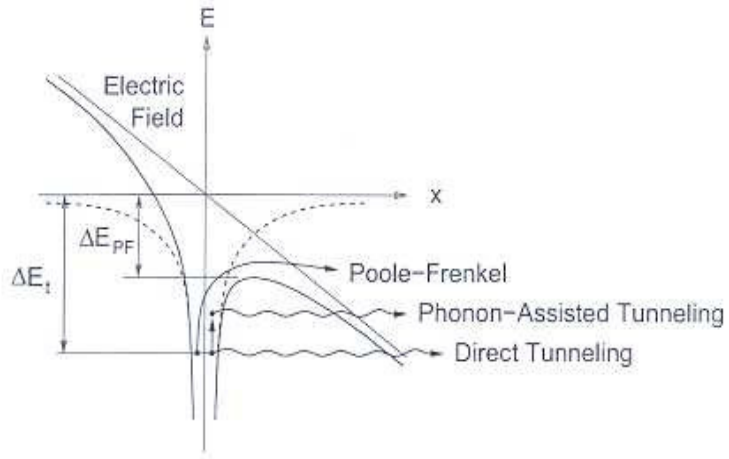

Fig. 2.15 *Field-enhanced emission mechanisms*

The other mechanisms shown in Fig. 2.15 are phonon-assisted tunnelling and direct tunnelling. These mechanisms favour the deeper-lying defects, with direct tunnelling mechanism being dominant in the high field regions (> 10^8 Vm^{-1}).

The phonon-assisted tunnelling mechanism occurs in defects with a significant electron-lattice coupling. Because of this coupling, the trapped defect can occupy a set of stationary quasi-levels separated by $\hbar\omega$, where $\hbar\omega$ is the phonon energy. From these quasi levels, elastic tunnelling can then occur to the conduction band. The coupling constant is given by [65],

$$S = \frac{\Delta E}{\hbar\omega} \tag{2.74}$$

where ΔE is the vibrational energy loss.

The field emission rate due to phonon-assisted tunnelling is represented by [63],

$$e_f = \sum_p \Pi_p(\Delta_p)(1 - f_{1,p}) \tag{2.75}$$

where $(1 - f_{1,p})$ is the Fermi-Dirac probability of finding an empty conduction band state, $\Gamma(\Delta_p)$ is the tunnelling emission probability for an electron at a quasi level p with energy Δ_p above the ground state and Π_p is the probability of finding the electron at quasi level p.

The probability (Π_p) of finding the trapped electron at a given quasi-level $E_c - \Delta_p$, where $p = 0, \pm 1, \pm 2, ...$ may be calculated from [63];

$$\Pi_p = \left(1 - \exp^{-\hbar\omega/kT}\right) \sum_{n=0}^{+\infty} \exp^{-n\hbar\omega/kT} J_p^2\left(2\sqrt{S\left(n + \frac{1}{2}\right)}\right) \tag{2.76}$$

where J_p is a Bessel function of the first kind and n the integer number of phonons. This model is based on the assumption that the phonons have a single well-defined angular frequency ω.

References

[1] C. Kittel, Introduction to Solid State Physics, Wiley & Sons, New York, 1976.

[2] E.E Haller, Mat. Sci. Semcond. Proc. **9** (2006) 408

[3] S.M. Sze, Physics of Semiconductor devices, Wiley & Sons, Canada, 1981.

[4] S. Li, Semiconductor Physical Electronics, Springer, 2006.

[5] C. Kettel, Quantum Theory of Solids, Wiley & Sons, New York, 1963.

[6] L.C. Allen, Phys. Rev, **98** (1955) 93

[7] F. Herman, Proc. IRE, **43** (1955) 1703.

[8] J.C. Philips, Phys. Rev. **112** (1958) 685.

[9] R.A Smith, Semiconductors, 2nd ed., Cambridge University Press, London, 1979.

[10] R.T. Tung, Mater. Sci. Eng. R **35** (2001) 1.

[11] M. Sağlam, F.E. Cimilli, A. Türüt, Physica B **348** (2004) 397.

[12] Ö. F. Yüksel, Physica B **404** (2009) 1993.

[13] W. Mönch, Semiconductor Surf. And Interfaces, 2nd ed., Springer, Berlin 1995.

[14] B. Boyarby, H. Çetin, M. Kaya, E. Ayyildiz, Microelectron. Eng. **85** (2008) 721.

[15] R.D. Thomson, K.N. Tu, J. Appl. Phys. **53** (1982) 4285.

[16] J.H. Werner, H. Guttler, J. Appl. Phys. **69** (1991) 1522.

[17] S. Chand, J. Kumar, J. Appl. Phys. **82** (1997) 5005.

[18] H. Çetin, E. Ayyildiz, Semicond. Sci. Technol. **20** (2005) 625.

[19] R.T. Tung, Phys. Rev. B. **45** (1992) 13509.

[20] W. Schottky, Naturwissenschaften **26** (1938) 843.

[21] N.F. Mott, Proc. Camb. Phil. Soc. **34** (1938) 568.

[22] E. H. Rhoderick, Metal-Semiconductor Contacts, Clarendon, Oxford, 1978.

[23] H.A. Bethe, MIT Radiant. Lab. Rep. **43** (1942) 12.

[24] B.G. Streetman, Solid State Electronic Devices, 5th Ed. Prentice Hall, New Jersey (2000)

[25] R.T. Tung, Mater. Sci. Eng. R **35** (2001) 1.

[26] Ş. Karadeniz, M. Şahin, N. Touğluoğlu, H. Şafak, Semicond. Sci. Technol. **19** (2004) 91098.

[27] S. Acar, S. Karadeniz, N. Tuğluoğlu, A.B. Selçuk, M. Kasap, Appl. Surf. Sci. **233** (2004) 373.

[28] A. Gümüş, A. Türüt, N. Yalçin, J. Appl. Phys. **91** (2002) 245.

[29] W. Mtangi, F.D. Auret, C. Nyamhere, P.J. Janse van Rensburg, M. Diale, A. Chawanda, Physica B **404** (2009) 1092.

[30] http://en.wikipedia.org/wiki/annealing_(metallurgy), 19/04/2010.

[31] M.G. Grimaldi, L. Wieluński, and M.-A. Nicolet, Thin Solid Films, **81** (1981) 207.

[32] H. Doğan, N. Yildirim, A. Türüt, Microelectron. Eng. **85** (2008) 655.

[33] Y. Sun, X.M. Shen, J. Wang, D.G. Zhao, G. Feng, Y. Fu, S.M. Zhang, Z.H. Zhang, Z.H. Feng,Y.X. Bai, H.Yang, J. Phys. D: Appl. Phys. **35** (2002) 2648.

[34] Q. Zhang, N. Wu, T. Osipowicz, L.K. Bera, C. Zhu, Jan. J. Appl. Phys. **44** (2005) L1389.

[35] J.P. Gambino, E.G. Colgan, Mater. Chem. Phys. **52** (1998) 99.

[36] P. Jayavel, K. Asokan, D. Kanjilal, J. Kumar, Mater. Sci. Semicond. Proc. **3** (2000) 195.

[37] F.D. Auret, W.E. Meyer, S. Coelho, and M. Hayes, Appl. Phys. Lett. **88** (2006) 242110.

[38] M.W. Thompson, Defects and Radiation Damage in Metals, Cambridge University Printing House, (1969) 11.

[39] M. Lannoo and J. Bourngoin, Point Defects in Semiconductors I, Theoretical Aspects Springer series in Solid State science 22 (1981).

[40] S.A. Centoni, B. Sadigh, G.H. Gilmer, T.J. Lenosky, T.D. de la Rubia, C.B. Musgrave, Phys. Rev**. B 72** (2005) 195206.

[41] A.R. Peaker, V.P. Markevich, F.D. Auret, L. Dobaczewski and N. Abrosimov, J.Phys. Condens. Matter **17** (2005) S2293.

[42] C.E. Linbergy, J. L. Hansen, P. Bomholt, A. Mesli, K. B. Nielsen, A. N. Lasen, L. Dobaczewski, Appl. Phys Lett. **87** (2005) 172103.

[43] J. Fage-Pedersen, A. Nylandsted Lartsen, and A. Mesli, Phys. Rev. B **62** (2001) 10116.

[44] V.P. Markevich, A.R. Peaker, V.V. Litvinov, V.V. Emstsev, and L.I. Murin, J. Appl. Phys. **95** (2004) 4078.

[45] V.P. Markevich, A.R. Peaker, L.I. Murin and N.V. Abrosimov, J.Phys.:Condens. Matter **15** (2003) S2835.

[46] V.P. Markevich, V.V. Litvinov, L. Dobaczewski, J.L. Lindström, L.I. Murin, S.V. Vetrov, I.D. Hawakins, A.R. Peaker, Physica B **340-342** (2003) 844.

[47] G.D. Watkins, J.W. Corbett, Phys. Rev. **121** (1961) 1001.

[48] V.P. Markevich, et al., Phys. Stat. Sol. (c) **0** (2003) 702.

[49] V.P. Markevich, et al., Appl. Phys. Lett. **81** (2002) 1821.

[50] D.V. Lang, J. Appl. Phys. **45** (1974) 3023.

[51] W. Shockley, W.T. Read, Phys. Rev. **87** (1952) 835.

[52] R.N. HallPhys. Rev. **87** (1952) 387.

[53] J. Bourgoin, M. Lannoo, Point defects in semiconductors II, Berlin: Springer (1983).

[54] G.L. Miller, D.V. Land, L.C. Kimerling, Ann. Rev. Mater. Sci. **7** (1977) 377

[55] F.D. Auret and P.N.K. Deenapanray, Crit. Rev. Sol. Stat. Mater. Sci. **29** (2004) 4689.

[56] L. Dobaczewski, A.R. Peaker and K.B. Nielsen, J. Appl. Phys. **96** (2004) 4689.

[57] V.P. Markevich, I.D. Hawkins, A.R. Peaker, K.V. Emtse, V.V. Litvinov, L.I. Murin, and L. Dobaczewski, Phys. Rev. B **70** (2004) 235213.

[58] Y.Zohta and M.O. Watanabe, J. Appl. Phys. **53** (1982) 1809.

[59] D.V. Lang, In "Thermally Stimulated Relxation of Solids" (P. Braunlich, ed.), Springer-Verlag, Berlin 1979.

[60] L. Dobaczewski, P. Kaczor, I.D. Hawkins and A.R. Peaker, J. Appl. Phys. **76** (1994) 194.

[61] D.K. Schroder, Semiconductor Material and Device Characterization, Wiley & Sons,2006.

[62] H. Lefevre and M. Schulz, J. Appl. Phys. 12 (1977) 45.

[63] D. Pons and S. Makran-Ebeid, J. Phys. **40** (1979) 1161.

[64] J. Frenkel, Phys. Rev. **54** (1938) 657.

[65] S. Makram-Ebeid and M. Lannoo, Appl. Phys. Lett. **37** (1980) 464.